

## Support Information for

### Super-paramagnetic nano-architecture for visible-light-driven Hydrogen Evolution

State Key Laboratory for Oxo Synthesis and Selective Oxidation, Lanzhou Institute of Chemical Physics, Chinese Academy of Sciences, Lanzhou, 730000, China.  
College of Material Engineering, Jinling Institute of technology, Nanjing, China

\*Corresponding author: E-mail: [gxlu@lzb.ac.cn](mailto:gxlu@lzb.ac.cn)

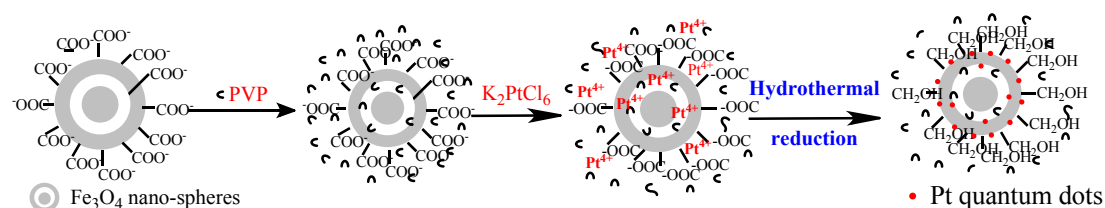
### Experimental details

#### Preparation of $Fe_3O_4$ micro-spheres

The mono-dispersed  $Fe_3O_4$  micro-spheres were synthesized by a one-pot hydrothermal method. In a typical synthesis,  $FeCl_3 \cdot 6H_2O$  (0.54 g), sodium citrate (1.2 g), and urea (0.2 g) were dissolved in distilled water (40 mL). Then, PAAS (0.2 g) was added under continuous stirring until it was totally dissolved. The solution was transferred to a 50 mL Teflon-lined autoclave, which was then sealed and maintained at 200°C for 12 h. The product was separated by magnetic separation, washed with distilled water and absolute ethanol several times, and then dried in a vacuum oven at 60 C overnight.

#### Preparation of $Fe_3O_4@Pt$ catalysts

The  $Fe_3O_4@Pt$  catalysts were synthesized by hydrothermal method, as shown in scheme 1. In a typical synthesis, 0.2 g prepared  $Fe_3O_4$  micro-spheres and 0.2 g poly(N-vinylpyrrolidone) (PVP) ( $K_{30}$ ) were re-dispersed into 40 mL distilled water via ultrasound. Under vigorous stirring, 0.6 g sodium citrate was dissolved into the above-prepared solution. Then 1 mL aqueous  $K_2PtCl_6$  (Pt: 2 mg/mL) was added into above solution subsequently. The solution was transferred to a 50 mL Teflon-lined autoclave, which was then sealed and maintained at 200°C for 12 h. The product was separated by magnetic separation, washed with distilled water and absolute ethanol several times, and then dried in a vacuum oven at 60°C overnight.

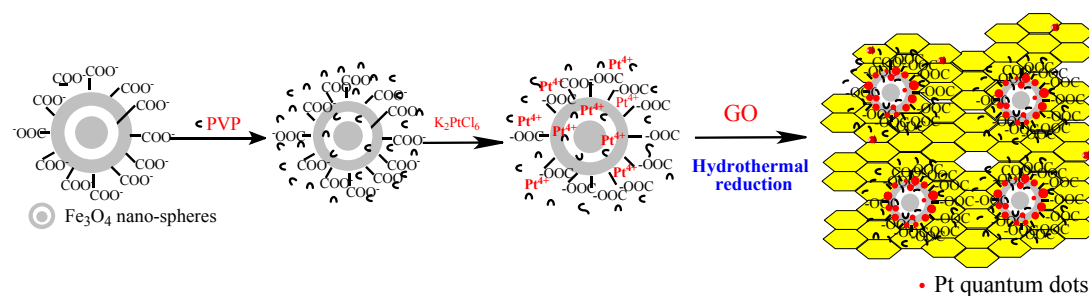


Scheme 1 Synthesis route of  $Fe_3O_4@Pt$  catalysts

#### Preparation of $Fe_3O_4@Pt@RG$ catalysts

The  $Fe_3O_4@Pt$  catalysts were synthesized by hydrothermal method, as shown in scheme 2. In a typical synthesis, 0.2 g prepared  $Fe_3O_4$  micro-spheres and 0.2 g poly(N-vinylpyrrolidone) (PVP) ( $K_{30}$ ) were re-dispersed into 40 mL distilled water via ultrasound. Under vigorous stirring, 1.2 g sodium citrate was dissolved into the above-prepared solution. Then 1 mL aqueous  $K_2PtCl_6$  (Pt: 2 mg/mL) and 2 mL graphene oxide (GO) solution (1mg/mL) was added into above solution subsequently. The solution was transferred to a 50 mL Teflon-lined autoclave, which was then

sealed and maintained at 200°C for 12 h. The product was separated by magnetic separation, washed with distilled water and absolute ethanol several times, and then dried in a vacuum oven at 60°C overnight.



**Scheme 2** Synthesis route of  $\text{Fe}_3\text{O}_4@\text{Pt}@\text{GO}$  catalysts

### ***Preparation of Pt@GR catalysts***

The Pt@GR catalysts were also synthesized by hydrothermal method. In a typical synthesis, 0.6 g sodium citrate was dissolved into 40 mL distilled water via ultrasound. Then 1 mL aqueous  $\text{K}_2\text{PtCl}_6$  (Pt: 2 mg/mL) and 2 mL graphene oxide (GO) solution (1mg/mL) was added into above solution subsequently. The solution was transferred to a 50 mL Teflon-lined autoclave, which was then sealed and maintained at 200°C for 12 h. The product was separated by magnetic separation, washed with distilled water and absolute ethanol several times, and then dried in a vacuum oven at 60°C overnight.

## **Characterization Details**

Transmission electron microscopy (TEM) and high-resolution TEM (HRTEM) were taken with a Tecnai-G2-F30 field emission transmission electron microscope operating at an accelerating voltage of 300 kV. X-ray diffraction (XRD) patterns of the samples were recorded on a Rigaku B/Max-RB diffractometer with a nickel filtered  $\text{Cu K}\alpha$  radiation operated at 40 kV and 40mA. X-ray photoelectron spectroscopy (XPS) analysis was performed using a VG Scientific ESCALAB210-XPS photoelectron spectrometer with an  $\text{Mg K}\alpha$  X-ray resource. Thermogravimetric analysis (TG) was performed in air using a Pyris Diamond TG analyzer (PerkinElementer Inc., U. S. A.). The diffuse reflectance spectra were collected on a Shimadzu UV-3101PC spectrophotometer with an integrating sphere.

FT-IR spectra were measured on a Nexus 870 FT-IR spectrometer from KBr pellets as the sample matrix. The fluorescence decay time were measured using the Horiba Jobin Yvon Data Station HUB operating in time-correlated single photon counting mode (TCSPC) with the time resolution of 200 ps. Nano LED diode emitting pulses at 460 nm with 1 MHz repetition rate was used as an excitation source.

The amount of hydrogen evolution was measured using gas chromatograph (Aglient 6820, TCD, 13×column, Ar carrier). The apparent quantum efficiency (AQE) was measured under the same photocatalytic reaction conditions with irradiation light through a band-pass filter (430, 460, 490, 520, or 550nm). Photon flux of the incident light was determined using a Ray virtual radiation actinometer (FU 100, silicon ray detector, light spectrum, 400-700 nm; sensitivity,  $10\text{-}50 \mu\text{V} \mu\text{mol}^{-1}\cdot\text{m}^2\cdot\text{s}^{-1}$ ).

The reactant mixture of EY-Ru was irradiated for 30 min by a 300-W Xe lamp with a cutoff filter of 420 nm and a bandpass filter for AQEs tests on the  $\text{H}_2$  production. The following equation (1) was used to calculate the AQE.

$$AQEs = \frac{2 \times \text{the number of evolved hydrogen molecules}}{\text{the number of incident photons}} \times 100\% \quad (1)$$

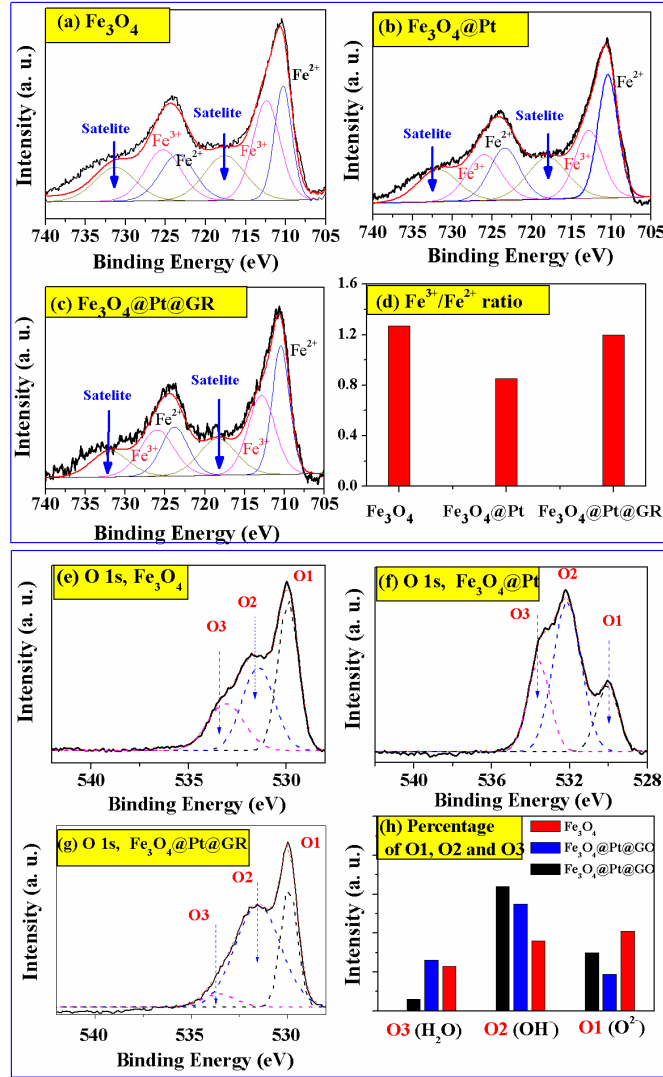


**Fig. S1 (a-d) Fe 2p scan spectra and (e-h) O 1s scan spectra of Fe<sub>3</sub>O<sub>4</sub>, Fe<sub>3</sub>O<sub>4</sub>@Pt and Fe<sub>3</sub>O<sub>4</sub>@Pt@GR**

The effect of GR on the e<sup>-</sup>-h<sup>+</sup> separation may not be the only reason for the enhancement of H<sub>2</sub> evolution. The surface states could also affect the efficiency of H<sub>2</sub> evolution. In **Fig. S1(a-d)**, the Fe<sub>2p<sub>1/2</sub></sub> and Fe<sub>2p<sub>3/2</sub></sub> peaks can be de-convoluted by six peaks around 710, 712, 718, 723, 725 and 732 eV. The two satellite peaks around 718 and 732 eV could be assigned to Fe<sup>3+</sup> in the Fe<sub>2</sub>O<sub>3</sub> phase, indicating that the surface of microspheres are slightly oxidized in the air environment. The other four peaks respectively correspond to the Fe<sup>2+</sup> (710, 723 eV) and Fe<sup>3+</sup> (712, 725 eV) in the Fe<sub>3</sub>O<sub>4</sub> phase. Area ratio of the Fe<sup>3+</sup>/Fe<sup>2+</sup> in Fe<sub>3</sub>O<sub>4</sub> phase were calculated to be 1.27/1, 0.90/1 and 1.20/1 for the Fe<sub>3</sub>O<sub>4</sub>, Fe<sub>3</sub>O<sub>4</sub>@Pt, and Fe<sub>3</sub>O<sub>4</sub>@Pt@GR (**Fig. S1 (d)**). The Fe<sup>3+</sup>/Fe<sup>2+</sup> ratio on Fe<sub>3</sub>O<sub>4</sub>@Pt surface deviates seriously from that on the surface of Fe<sub>3</sub>O<sub>4</sub>. The result indicates lots of surface defects existing on the surface of Fe<sub>3</sub>O<sub>4</sub>@Pt.

As for the Fe<sub>3</sub>O<sub>4</sub>@Pt@GR, the Fe<sup>3+</sup>/Fe<sup>2+</sup> ratio on its surface revives back to 1.20/1. The decreasing of Fe<sup>3+</sup>/Fe<sup>2+</sup> ratio indicates that the GR could “repair” or “cover” the surface defects of Fe<sub>3</sub>O<sub>4</sub> microspheres. The protection effect of graphene has also been found for improving the cycle performance of SnO<sub>2</sub>-GR electrodes<sup>[S1]</sup>. As a result, application efficiency of the photo-generated charges could be improved because more photo-electrons were separated and transferred to the co-catalysts before quenched by the surface defects. In order to investigate

the effect of Fe<sub>3</sub>O<sub>4</sub> on the performance of hydrogen evolution, the hydrogen evolution rate over Pt@GR was also collected and compared with that of Fe<sub>3</sub>O<sub>4</sub>@Pt@GR (Fig. S11). H<sub>2</sub> evolution over the Fe<sub>3</sub>O<sub>4</sub>@Pt@GR was lower than that over the Pt@GR, indicating that some photo-electrons were quenched by the defects on the Fe<sub>3</sub>O<sub>4</sub> surface.

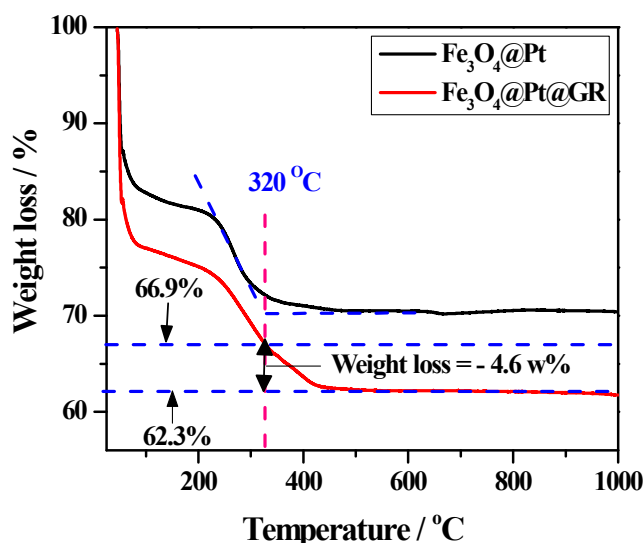


Fig. S2 the TG curve of Fe<sub>3</sub>O<sub>4</sub>@Pt microspheres and Fe<sub>3</sub>O<sub>4</sub>@Pt@GR

As shown in Fig. S2, the TG curve of Fe<sub>3</sub>O<sub>4</sub>@Pt microspheres shows two weight loss processes. The weight loss below 100 °C can be attributed to the loss of absorbed water. The rapid mass loss between 100-320 °C can be attributed to the organic groups (citrate and poly-acrylic groups) and residual PVP adhered on the Fe<sub>3</sub>O<sub>4</sub> microspheres. As for the Fe<sub>3</sub>O<sub>4</sub>@Pt@GR, the mass loss between 320-550 °C is related to the oxidation of carbon [S2]. With the enhancement of temperature, the GR gradually decomposed. According to the TG curve, the percentage of graphene in the composites is about 7%.

The residual weight of Fe<sub>3</sub>O<sub>4</sub>@Pt@GR is about 61.6% after 1000 °C. In fact, the Fe<sub>3</sub>O<sub>4</sub> was oxidized to be Fe<sub>2</sub>O<sub>3</sub> at air atmosphere when temperature is higher than 550 °C [S3]. The residual product after 1000 °C is the Fe<sub>2</sub>O<sub>3</sub> and Pt particle. As the weigh increase is little when the Fe<sub>3</sub>O<sub>4</sub> is oxidized ( $\text{Fe}_3\text{O}_4 + 1/4\text{O}_2 = 3/2\text{Fe}_2\text{O}_3$ , weigh increase = 1.72%), the real amount of Fe<sub>3</sub>O<sub>4</sub> and Graphene in the prepared samples could be roughly calculated as follows:

$$\text{Weight ratio of } \text{Fe}_3\text{O}_4 : \text{GR} = \frac{62.3\% * \frac{15}{15+1}}{4.6\%} = 12.7$$

The weight ratio of Fe<sub>3</sub>O<sub>4</sub> to Graphene (GR) is a little lower than that to the graphene oxide (GO). That may be due to the reduction of hydroxyl, and carbonyl, carboxyl and other oxygen groups on the GO sheets.

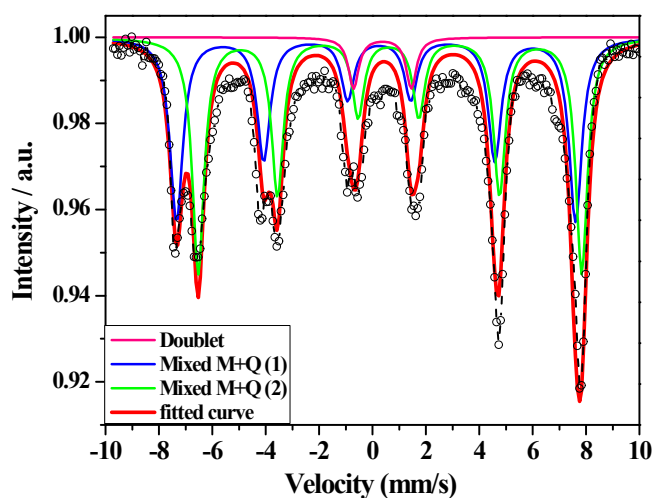


Fig. S3 Mössbauer spectra of Fe<sub>3</sub>O<sub>4</sub> microspheres at room temperature

**Table S1** Hyperfine parameters extracted from Mössbauer spectra at room temperature: isomer shift (IS), quadrupolar splitting (QS), hyperfine field ( $B_{\text{hyp}}$ ), and relative spectral area (I) for Fe<sub>3</sub>O<sub>4</sub> nanoparticles

Species	IS (mm/s)	QS (mm/s)	H (T)	I(%)
Fe <sup>3+</sup> ions in A sites	0.19	-0.12	46.46	43.7 %
Fe <sup>2.5+</sup> ions in B sites	0.63	0.056	44.64	51.5 %
Doublet (1)	0.375	2.16		4.8 %

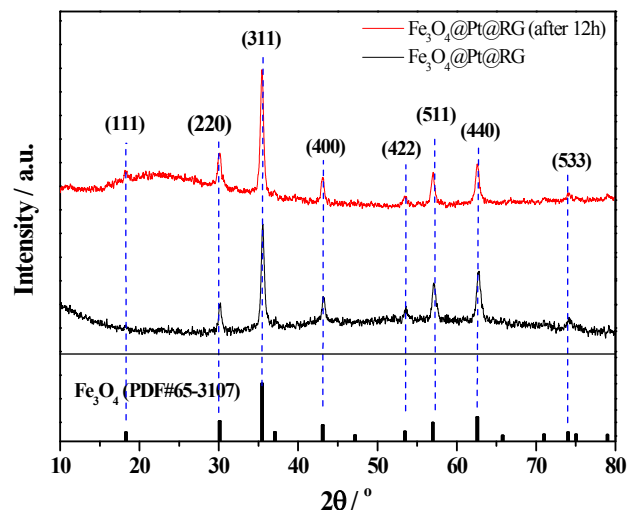
IS: isomer shift; QS: quadrupole shift; H: hyperfine magnetic field in Tesla  
A sites: tetrahedral sites. B sites: octahedral sites.

Figure S3 shows Mössbauer spectrum of the magnetic catalysts at room temperature. The spectrum could be fitted by two magnetic sextets, which corresponds to the Fe<sup>3+</sup> ions at site A (tetrahedral site) and the Fe<sup>“2.5+”</sup> ions at site B (octahedral site) in the Fe<sub>3</sub>O<sub>4</sub> phase [S4-S6], respectively. Fe<sup>“2.5+”</sup> corresponds to the average signal of Fe<sup>2+</sup> and Fe<sup>3+</sup> located in the octahedral sites. There exists fast electron exchange between the two ions when the temperature is higher than 260 K. Table 1 shows the hyperfine parameters calculated from the Mössbauer spectrum. The stoichiometry of the catalyst is calculated to be Fe<sub>2.94</sub>O<sub>3</sub>. The stoichiometry of the catalyst was determined by the following formula<sup>[S5]</sup>:

$$X = \frac{2 - 1.1 * R}{6 + 4.945 * R}$$

$$R = \frac{\text{Relative population of Fe}^{2.5+} \text{ in octahedral sites}}{\text{Relative population of Fe}^{3+} \text{ in tetrahedral sites}}$$

X = oxidation parameter according with Fe<sub>3-x</sub>O<sub>4</sub> formula



**Fig. S4 The XRD patterns of  $\text{Fe}_3\text{O}_4@\text{Pt}@\text{GR}$  photo-catalyst before and after 12 h photo-catalytic reaction**

Fig. S4 shows the XRD patterns of  $\text{Fe}_3\text{O}_4@\text{Pt}@\text{GR}$  photo-catalyst before and after 12 h photo-catalytic reaction. After 12 h photo-catalytic reaction, the diffraction peaks of  $\text{Fe}_3\text{O}_4@\text{Pt}@\text{GR}$  still correspond to the crystal planes of cubic  $\text{Fe}_3\text{O}_4$  (JCPDS#65-3107). It indicates that the crystal structure of  $\text{Fe}_3\text{O}_4$  remained well after 12 h reaction. Fig. S5 shows the morphology of  $\text{Fe}_3\text{O}_4@\text{Pt}@\text{GR}$  after 12 h catalytic reaction.

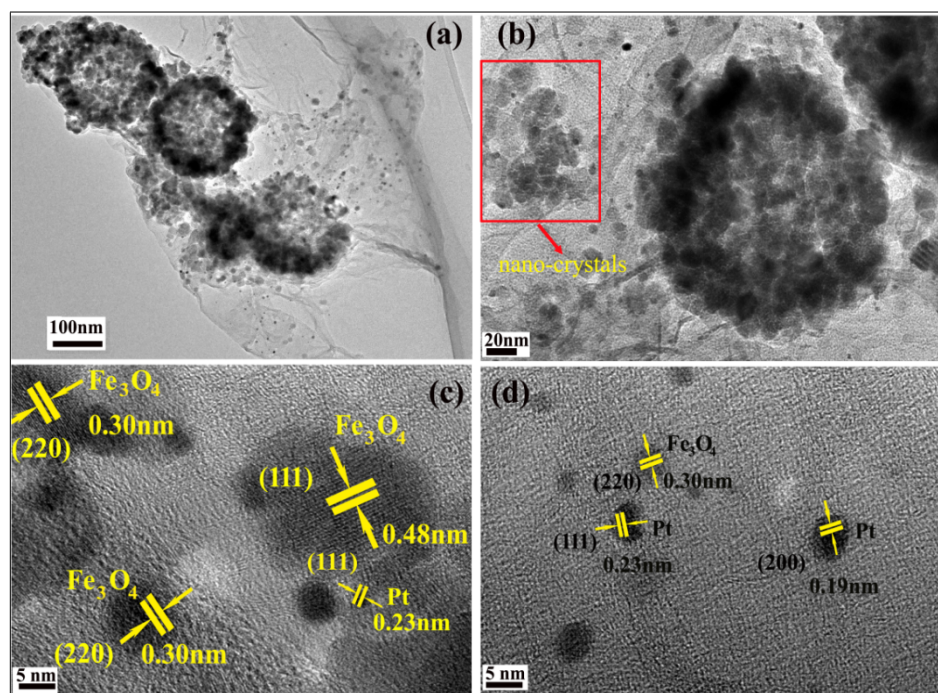


**Fig. S5 TEM image (a, b) and HRTEM image (c, d) for  $\text{Fe}_3\text{O}_4@\text{Pt}@\text{GR}$  (after 12 h photo-catalytic reaction)**

Before photo-catalytic reaction, the  $\text{Fe}_3\text{O}_4$  microspheres on  $\text{Fe}_3\text{O}_4@\text{Pt}@\text{GR}$  are assembled by lots of  $\text{Fe}_3\text{O}_4$  nano-crystals which linked by sodium polyacrylate (Fig. 1). After 12 h reaction, some  $\text{Fe}_3\text{O}_4$  microspheres were partially broken and plenty of  $\text{Fe}_3\text{O}_4$  nano-crystals were released from the microspheres (Fig. S5(a, b)). Some  $\text{Fe}_3\text{O}_4$  nano-crystals deposit on the GR sheets and expose large surface area (Fig. S5 (c, d)).

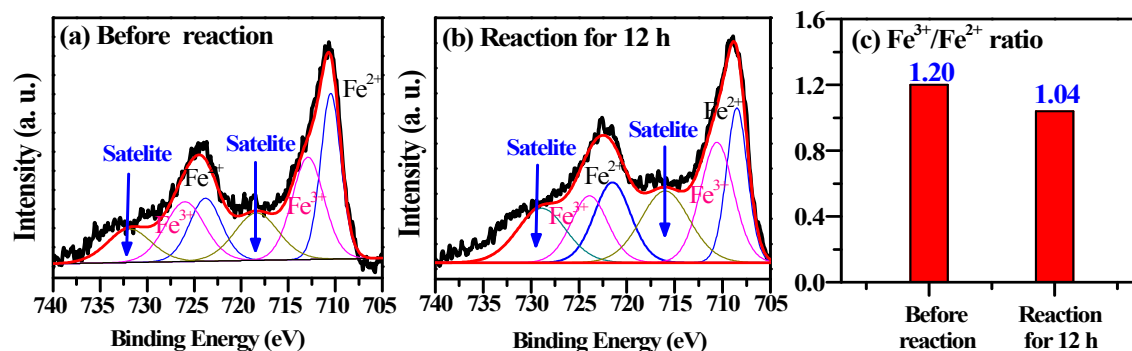


Fig. S6 Fe 2p scan spectra of Fe<sub>3</sub>O<sub>4</sub>@Pt@GR (a) before and (b) after 12 h reaction

XPS spectra were also recorded to reveal more information for the degradation of catalytic activity after 140 min reaction. After 12 h reaction, the Fe<sup>3+</sup>/Fe<sup>2+</sup> area ratio on Fe<sub>3</sub>O<sub>4</sub>@Pt@GR surface deviates seriously from that before the photo-catalytic reaction. The result indicates lots of surface defects were formed on the surface of Fe<sub>3</sub>O<sub>4</sub>@Pt@GR. It is not difficult to understand the result according to the mechanism of dye-sensitized H<sub>2</sub> evolution. Upon visible light irradiation, the electrons at the highest-occupied molecular orbital (HOMO) of Eosin Y (EY) absorbs light photon and be excited to the lowest-unoccupied molecular orbital (LUMO). Then the excited electron of EY could be transferred to the catalyst for H<sub>2</sub> evolution. Inevitably, some photo-generated electrons may be quenched by the defects on Fe<sub>3</sub>O<sub>4</sub> surface. Some Fe<sup>3+</sup> ions on the surface of catalyst were then reduced to be Fe<sup>2+</sup> ions by the excited electrons, as a result decreasing the ratio of Fe<sup>3+</sup>/Fe<sup>2+</sup> on the surface of catalyst.

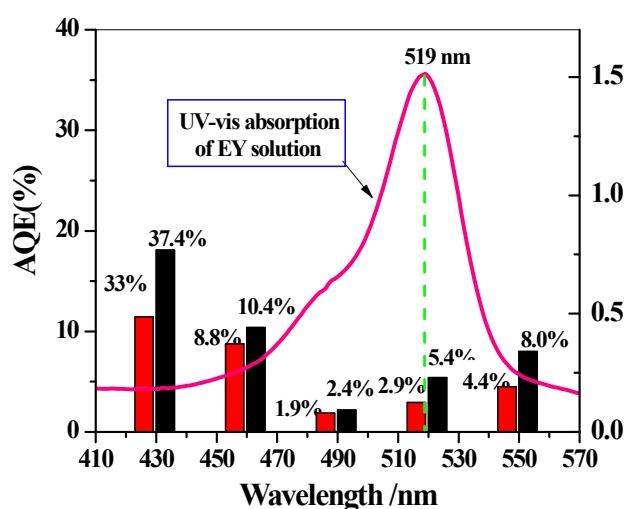


Fig. S7 UV-vis absorption of EY solution ( $1.0 \times 10^{-3}$  mol/L)

The maximum absorption wavelength of EY dye is 519 nm in this reactive system. The increase of AQE at 520 nm is due to the strong absorption of EY dye for the 519 nm light [S7-S9].

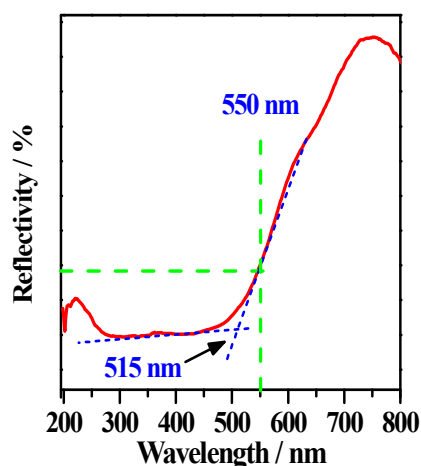


Fig. S8 UV-visible diffuse reflection spectra of  $\text{Fe}_3\text{O}_4@\text{Pt}@\text{GR}$  powders

As shown in Fig. S8, the  $\text{Fe}_3\text{O}_4@\text{Pt}@\text{GR}$  catalyst exhibits broad absorption band at 300-500 nm regions. The strong and broadband absorption for visible light is due to the d-d  $\text{Fe}^{3+}$  ligand field transitions<sup>[S10]</sup>. The photos absorbed by  $\text{Fe}_3\text{O}_4$  could not be applied by the EY dye to excite the photo-generated electrons. As a result, the apparent quantum efficiency decreased at 450 and 490 nm. Fig. S8 also shows that the photo-absorption of  $\text{Fe}_3\text{O}_4$  decreased for the lights longer than 515 nm. The increase of AQE at 550 nm could be attributed to low photo-absorption of  $\text{Fe}_3\text{O}_4$  for 550 nm light.

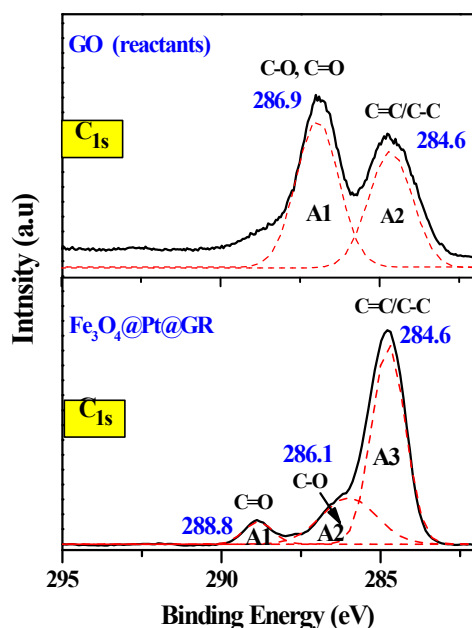
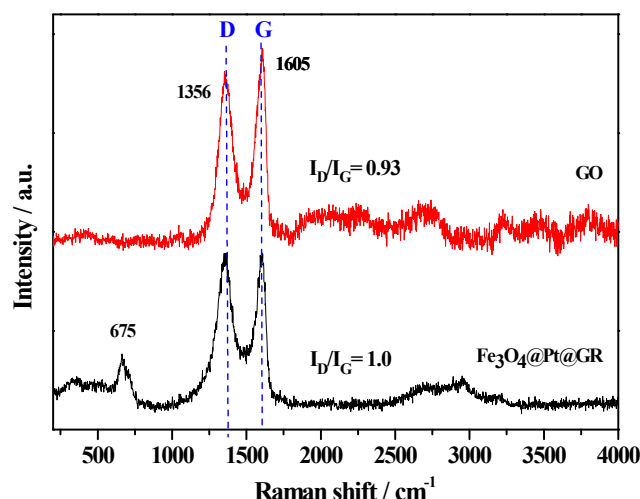


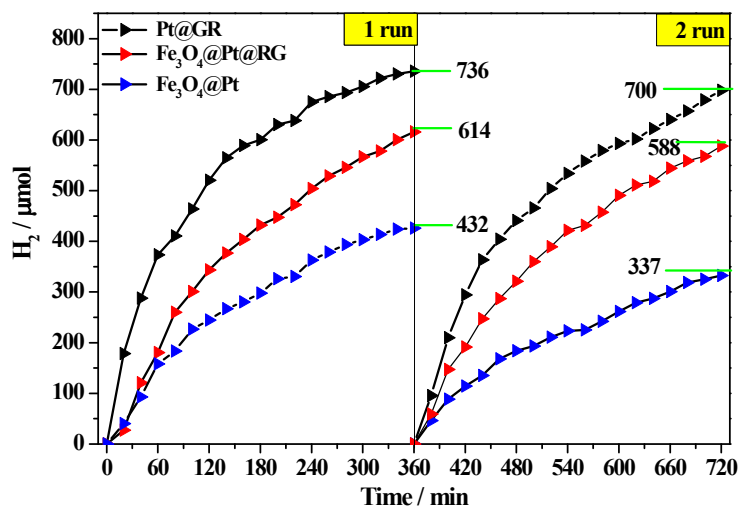
Fig. S9  $\text{C}_{1s}$  scan spectra of (a) raw GO for hydrothermal reaction and (b)  $\text{Fe}_3\text{O}_4@\text{Pt}@\text{GR}$

Fig. S9 shows the  $\text{C}_{1s}$  scan spectra of raw GO and the prepared  $\text{Fe}_3\text{O}_4@\text{Pt}@\text{GR}$  catalyst. The  $\text{C}_{1s}$  spectrum of GO can be deconvoluted into two peaks at 284.6 and 286.9 eV, which could be assigned to the  $\text{sp}^2$ -hybridized C ( $\text{C}=\text{C}-\text{C}$ ) and the C in oxygen-containing functional groups ( $\text{C}-\text{O}/\text{C}=\text{O}$ ), respectively<sup>[S11]</sup>. The  $\text{Fe}_3\text{O}_4@\text{Pt}@\text{GR}$  has much less oxygen-containing groups than the raw GO. The  $\text{C}_{1s}$  scan spectra indicate that most of the oxygen-containing groups have been reduced during the hydrothermal reaction. The raw GO was reduced to graphene (GR) by hydrothermal process.



**Fig. S10 Raman spectra of Graphene Oxide and  $\text{Fe}_3\text{O}_4@\text{Pt}@\text{GR}$**

Raman measurement was also characterized to investigate the structure of carbon material in the composite catalyst. The two distinct peaks at  $1356$  and  $1605$   $\text{cm}^{-1}$  could be assigned to the “D” and “G” band of carbon materials. The peaks at  $675$   $\text{cm}^{-1}$  could be assigned to the  $\text{Fe}_3\text{O}_4$ . The D band is assigned to the  $A_{1g}$  breathing mode of a disordered graphite structure, whereas the G band indicates the presence of the  $E_{2g}$  structure mode of crystalline graphite ( $\text{sp}^2$  hybridized carbon). The intensity ratio of D to G band ( $I_D/I_G$ ) increased from 0.93 to 1.0 when the raw GO is reduced to  $\text{Fe}_3\text{O}_4@\text{Pt}@\text{GR}$  during the hydrothermal process. The increase of  $I_D/I_G$  could be attributed to the formation of new, smaller  $\text{sp}^2$  domains during the reduction [S12]. It indicates that the conductive network of GO sheets has been repaired with small and isolated domains of aromatics within the sheets [S12, S13].



**Fig. S11  $\text{H}_2$  evolution from EY photosensitized systems ( $1.0 \times 10^{-3}$  mol/L) in 100 mL of 10% (v/v) TEOA aqueous solution ( $\text{pH}=11$ ,  $\lambda \geq 420$  nm).**

Fig. S11 shows the  $\text{H}_2$  evolution over the  $\text{Pt}@\text{GR}$ ,  $\text{Fe}_3\text{O}_4@\text{Pt}@\text{GR}$  and  $\text{Fe}_3\text{O}_4@\text{Pt}$ . Compared with the  $\text{Fe}_3\text{O}_4@\text{Pt}@\text{GR}$ , the  $\text{Pt}@\text{GR}$  exhibits higher  $\text{H}_2$  evolution in each run, indicating that some photo-electrons were quenched by defects on the  $\text{Fe}_3\text{O}_4$  surface. The  $\text{Pt}@\text{GR}$  catalyst was separated by centrifugation while the  $\text{Fe}_3\text{O}_4@\text{Pt}@\text{GR}$  and  $\text{Fe}_3\text{O}_4@\text{Pt}$  catalysts were separated by magnetic induction. In the second run, the  $\text{H}_2$  evolution over  $\text{Pt}@\text{GR}$  degrades from 736 to 700  $\mu\text{mol}$ . The dropping of hydrogen evolution is mainly due to the weight loss of  $\text{Pt}@\text{GR}$  during the centrifugal separation.

## Reference

- [S1] J. Zhu, G. Zhang, X. Yu, Q. Li, B. Lu, Z. Xu, *Nano Energy* 2014, 3, 80
- [S2] D. Chen, G. Wang, S. He, J. Liu, L. Guo, M. Cao, *J. Mater. Chem. A*, 2013, 1, 5996.
- [S3] A. Jafari, S. Farjami Shayesteh, M. Salouti, K. Boustani, *J. Magnetism and Magnetic Mater.*, 2015, 379, 305.
- [S4] C. Jin, Y. Wang, H. Tang, H. Wei, X. Liu, J. Wang, *J. Phys. Chem. C* 2014, 118, 25110
- [S5] C. Jin, Y. Wang, H. Wei, H. Tang, X. Liu, T. Lu, J. Wang, *J. Mater. Chem. A*, 2014, 2, 11202
- [S6] M. Yharour, N. Fellenz, A. Alvarez, J. Bengoa, N. Gallegos, M. Cagnoli, S. Marchetti, 2014, 39, 12563.
- [S7] S. Min, G. Lu, *J. Phys. Chem. C*, 2012, 116, 25415–25424
- [S8] C. Kong, S. Min, G. Lu, *ACS Catal.*, 2014, 4, 2763–2769
- [S9] C. Kong, S. Min, G. Lu, *Int. J. Hydrogen Energy*, 2014, 39, 4836.
- [S10] M. Yharour, N. Fellenz, A. Alvarez, J. Bengoa, N. Gallegos, M. Cagnoli, S. Marchetti, *Int. J. Hydrogen Energy*, 2014, 39, 12563.
- [S11] S. Saha, M. Jana, P. Samanta, N. Murmu, N. Kim, T. Kuila, J. Lee, *RSC Adv.*, 2014, 4, 44777.
- [S12] R. Nie, J. Wang, L. Wang, Y. Qin, P. Chen, Z. Hou, *Carbon*, 2012, 50, 586.
- [S13] D. Chen, G. Wang, S. He, J. Guo, M. Cao, *J. Mater. Chem. A*, 2013, 1.